






Calibration of the SHERLOC Deep Ultraviolet Fluorescence–Raman Spectrometer on the *Perseverance* Rover

Kyle Uckert¹ , Rohit Bhartia², Luther W. Beegle¹ ,
Brian Monacelli¹, Sanford A. Asher³, Aaron S. Burton⁴,
Sergei V. Bykov³, Kristine Davis⁴, Marc D. Fries⁴,
Ryan S. Jakubek⁵ , Joseph Razzell Hollis¹, Ryan D. Roppel³ ,
and Yen-Hung Wu¹

Applied Spectroscopy
2021, Vol. 75(7) 763–773
© The Author(s) 2021
Article reuse guidelines:
sagepub.com/journals-permissions
DOI: 10.1177/00037028211013368
journals.sagepub.com/home/asp


Abstract

We describe the wavelength calibration of the spectrometer for the scanning of habitable environments with Raman and luminescence for organics and chemicals (SHERLOC) instrument onboard NASA's *Perseverance* Rover. SHERLOC utilizes deep ultraviolet Raman and fluorescence (DUV R/F) spectroscopy to enable analysis of samples from the Martian surface. SHERLOC employs a 248.6 nm deep ultraviolet laser to generate Raman-scattered photons and native fluorescence emission photons from near-surface material to detect and classify chemical and mineralogical compositions. The collected photons are focused on a charge-coupled device and the data are returned to Earth for analysis. The compact DUV R/F spectrometer has a spectral range from 249.9 nm to 353.6 nm ($\sim 200\text{ cm}^{-1}$ to $12\,000\text{ cm}^{-1}$) (with a spectral resolution of 0.296 nm ($\sim 40\text{ cm}^{-1}$)). The compact spectrometer uses a custom design to project a high-resolution Raman spectrum and a low-resolution fluorescence spectrum on a single charge-coupled device. The natural spectral separation enabled by deep ultraviolet excitation enables wavelength separation of the Raman/fluorescence spectra. The SHERLOC spectrometer was designed to optimize the resolution of the Raman spectral region and the wavelength range of the fluorescence region. The resulting illumination on the charge-coupled device is curved, requiring a segmented, nonlinear wavelength calibration in order to understand the mineralogy and chemistry of Martian materials.

Keywords

Deep ultraviolet, DUV, Raman spectroscopy, Mars 2020, scanning habitable environments with Raman and luminescence for organics and chemicals, SHERLOC, calibration, fluorescence, organics, minerals

Date received: 14 February 2021; accepted: 2 April 2021

Introduction

NASA's *Perseverance* rover is a mobile robotic platform that landed on the surface of Mars on 18 February 2021. *Perseverance* will perform scientific research that explores an astrobiologically relevant ancient environment on Mars within the Jezero Crater landing site.¹ The scientific goals of the mission are to (i) explore an astrobiologically relevant ancient environment on Mars to decipher its geological processes and history, including the assessment of past habitability, (ii) assess the biosignature preservation potential and search for potential biosignatures, and (iii) demonstrate significant technical progress towards the future return of well-documented samples to Earth, selected for their

scientific value. Scanning habitable environments with Raman and luminescence for organics and chemicals

¹Jet Propulsion Laboratory California Institution of Technology, Pasadena, CA, USA

²Photon Systems, Inc., Covina, CA, USA

³University of Pittsburgh Chemistry Department, Pittsburgh, PA, USA

⁴NASA Johnson Space Center, Houston, TX, USA

⁵Jacobs Technology, Inc., Houston, TX, USA

Corresponding author:

Kyle Uckert, NASA Jet Propulsion Laboratory, 4800 Oak Grove Drive, Pasadena, CA 91109, USA.

Email: kyle.uckert@jpl.nasa.gov

(SHERLOC) is one of seven selected instruments as part of the Mars 2020 scientific payload.²

Located on the robotic arm of the rover, SHERLOC operates under ambient Martian conditions.^{3,4} SHERLOC combines microscopic images and spectral mapping ($\leq 100 \mu\text{m}/\text{mapping pixel}$) to generate a microscopic view of the spatial distribution and interaction between organics, minerals, and chemicals important to the assessment of potential biogenicity. This chemical and mineral map of the organic geochemistry of a target on Mars, when combined with results from other *Perseverance* instruments, such as Mastcam-Z,⁵ planetary instrument for X-ray lithochemistry (PIXL),³ and SuperCam,⁶ will enable analysis of geological materials for both scientific research and determination of which samples to collect and cache for Mars sample return.^{3,5,6} SuperCam is a combination laser-induced breakdown spectrometer (LIBS), reflectance spectrometer, and time-resolved luminescence and Raman spectrometer capable of stand-off measurements, with further details described in Wiens et al.⁶ Unlike SuperCam, SHERLOC uses a deep UV (DUV) source to generate hyperspectral maps of a target, revealing mineral and potential organic variability over a postage-stamp sized area.

Using a pulsed NeCu laser to generate 248.6 nm photons, SHERLOC generates Raman-scattered photons from organics and minerals as well as fluorescence emission from aromatic organic compounds.^{7,8} The peak positions of the Raman-scattered photons lead to classification of functional groups of chemical compounds within the volume illuminated by the laser. The assignment of mineral and organic

classes may be made through the analysis of Raman peak positions. To achieve this, the spectrometer was designed with a spectral resolution of $<0.310 \text{ nm}$ (50 cm^{-1}) in the Raman region. While the design specifications were in nanometers, Raman peak positions are reported as Raman shifts (in wavenumbers), which allows for more direct comparison with Raman spectra collected with different excitation wavelengths. The resultant range of the Raman region obtained by SHERLOC is ~ 800 to 4000 cm^{-1} with a resolution of $\leq 40 \text{ cm}^{-1}$.² The fluorescence region extends to 353.6 nm, with a resolution ranging from 0.3 to 0.55 nm, where the resolution decreases as a function of wavelength in this system, described in more detail in the Slit Width and Spectral Resolution section.

SHERLOC is mounted to a robotic arm, which positions the instrument $48 \text{ mm} \pm 7 \text{ mm}$ above the target. The autofocus and contextual imager (ACI), laser illumination, and spectroscopy collection paths all share the same objective lenses, and image the same target (i.e., all three paths are co-boresighted), as shown in Figs. 1 and 2. The ACI generates context images of the target ($16.2 \times 12.1 \text{ mm}$ area) with a pixel resolution of $10.1 \mu\text{m}/\text{pixel}$ ($\leq 1/10$ of the $\sim 100 \mu\text{m}$ laser beam diameter at the target). ACI images are used to determine the focus position of all three paths by moving a motorized objective lens through the optimum focus for the imager, laser, and spectrometer. Leveraging the narrow depth-of-field of the ACI, the optimum focus can be calculated from a focus stack of images.⁹ The three co-boresighted optical paths comprise the SHERLOC optical system (Figs. 1 and 2).

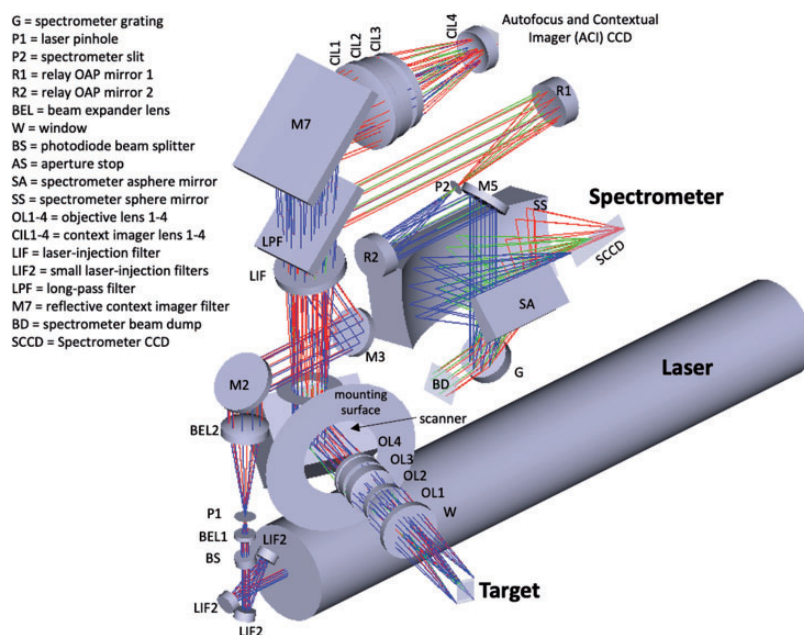


Figure 1. Ray trace of the SHERLOC optical path.² The laser photodiode is concealed by other components in this ray trace, but is displayed in Fig. 2.

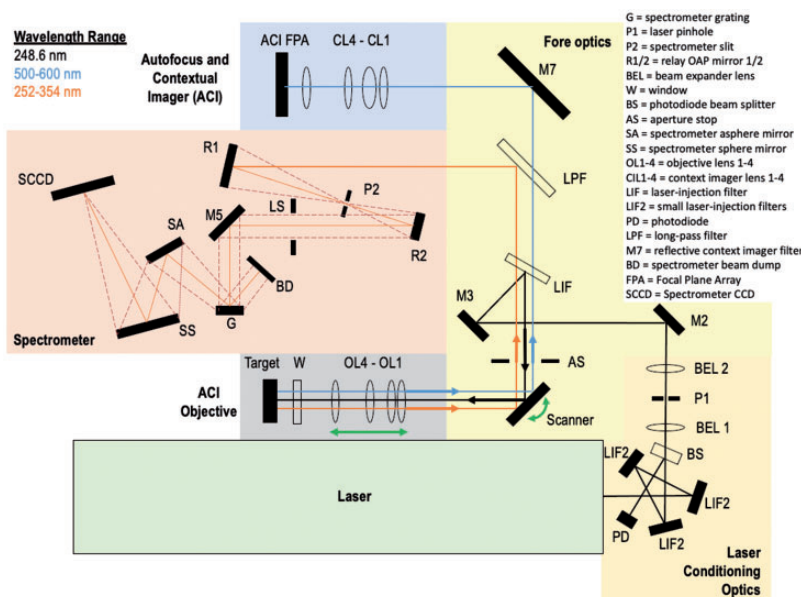


Figure 2. 2D block diagram of the SHERLOC optical path.²

When in focus, the objective lens focuses the laser to a 100–110 μm diameter spot. The nonuniform distribution of ions in the negative glow region of the NeCu laser leads to an annular, Laguerre–Gaussian mode.^{2,8} This annular feature will be re-imaged at the slit of the spectrometer and detector, with the re-imaged annulus shape dependent on the scattering properties of the target and the laser depth of penetration. The distribution of scattered light imaged on the detector affects the spectral fit applied to the narrow-band features. Raman peaks from weakly scattering targets are best fit by profiles that approach a flat-top Gaussian (modeled using a Fermi–Dirac distribution throughout this manuscript), and images resulting from high scattering and high depth of penetration will approach a Gaussian profile. As such, the SHERLOC calibration analysis was conducted with various Raman scattering samples.

Incident DUV laser pulses are focused on a target, using the moveable scanner mirror to sweep over an area to generate a map. The Raman and fluorescence photons excited by the laser are collected by the common-path ACI objective lens. The majority of the 248.6 nm laser line is rejected by a laser injection filter (LIF) with a 50% transmission point at 253.18 nm, which strongly reflects light <251 nm, as shown in Fig. 2. The Raman and fluorescence photons that pass through are injected into the SHERLOC spectrometer with a longpass filter (LPF) that transmits ≥ 400 nm light to the ACI. The 2D image of the distribution of Raman and fluorescence signal is de-magnified by 0.57 times from the target to the spectrometer’s slit, a 62.4×120.8 μm laser-drilled aperture. Assuming minimal scatter from the target, and considering the de-magnification, the 100 μm laser focal spot at the target measures at

57 μm at the slit. This sets the highest spectral resolution possible, which is limited by the slit. However, the 62.4 μm spectrometer slit width (along the spectral direction) sets the spectroscopy aperture. The slit, or the image at the slit, is then magnified by 1.29 times at the detector. Between the slit and the charge-coupled device (CCD), the SHERLOC spectrometer diffracts the Raman and fluorescence signal using a custom e-beam lithographically etched grating, enabling low scattering with a groove density of 4200 grooves per mm. The light is diffracted onto the spectrometer’s off-axis mirrors, which focus the dispersed spectral signal across the long axis of the 512×2048 pixel spectrometer CCD (SCCD), where each pixel is 13.5×13.5 μm . The off-axis nature of the spectrometer’s optical design causes a physical curving of the spectrum across the SCCD focal plane, which we refer to as a spectral “smile”. This smile is the byproduct of a compact spectrometer, use of reflective optics to limit chromatic aberrations, the fewest optics for high optical throughput, and optical forms that were low-risk and manufacturable with low surface roughness <5 \AA , and in a configuration that fit within the available volume on the robotic arm. The design was controlled to ensure that the Raman region was an optimized flat region of the illuminated curve on the detector, and occupied the fewest number of CCD rows to be binned to limit summing of dark charge. Additional details on the design and fabrication of SHERLOC may be found in Bhartia et al.²

Data are read out in a columnar fashion, typically using three binned regions, as shown in Fig. 3: Region 1 collects the Raman signal from 250 to 282 nm (225 to 4760 cm^{-1}), while Regions 2 and 3 collect fluorescence up to 355 nm.

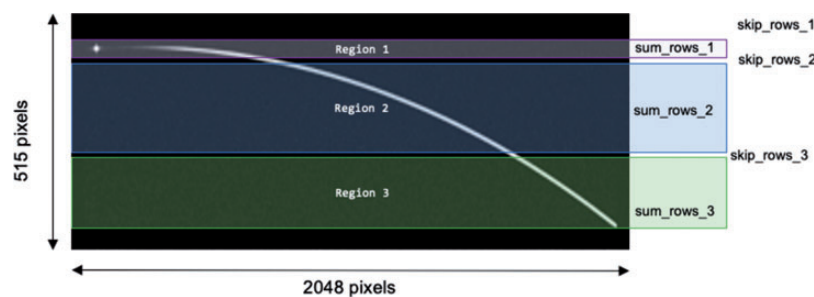


Figure 3. Illustration of the SCCD detector array overlaid with the spectrometer “smile” pattern and the on-chip integration patterns.²

Dividing the SCCD into multiple regions minimizes noise and allows for configurable clock speeds and variable gain settings. These variable gain settings provide the flexibility to change the electrons/count for a binned region to accommodate the dynamic range necessary to acquire both low Raman signals, and the relatively more intense fluorescence signals, which may saturate the detector if a single gain setting was applied across the entire SCCD. As indicated in Fig. 3, SCCD rows may be skipped to limit noise if hot pixels appear over time, but this feature is currently not in use. A 2D image of the SCCD may be downlinked to characterize hot pixels and to reduce noise in the spectrum by binning only light-sensitive pixels in each column of the SCCD.

Spectrometer Calibration Method

Slit Width and Spectral Resolution

The instrument was aligned using narrow mercury emission lines across the entire SHERLOC spectrum, and calibrated using the 253.65 nm mercury line to yield an instrument lineshape function of <5 pixels full width at half-maximum (FWHM) in the Raman region. The optical design specifies a spectral resolution of ≤ 0.310 nm in the Raman region, and performance was measured at 0.269 nm. While the spectrometer is reflective, the off-axis optical system creates a wavelength-dependent resolution since the image of the slit rotates to subtend more pixels at longer wavelengths. Therefore, when binning SCCD rows, the spatial height of the slit effectively increases the apparent slit width and thus reduces the spectral resolution at longer wavelengths. The slit image size ranges in width from 58 μm in the Raman region to 101 μm in the fluorescence region. Given the nature of the interpretation of fluorescence spectra, which does not generally rely on the assignment of narrow-band peaks, the resulting increase in spectral width at longer wavelength has negligible consequence.

As described in the Introduction, the SHERLOC annular laser beam underfills the slit. Assuming that the linewidth of the observed band is less than the spectrometer bandwidth, and that the Raman or fluorescence image of the target is

low scattering, the resulting lineshape, when binned, is a non-Gaussian beam profile that is best represented by a Fermi–Dirac profile,¹⁰ as described in Eq. 1

$$y(x) = \frac{H_0}{1 + e^{\frac{|x-x_0| - W}{R}}} \quad (1)$$

where $y(x)$ represents the spectral intensity and H_0 represents the maximum peak intensity. In the numerator of the exponential ($|x-x_0| - W$), x represents the CCD channel number, x_0 represents the peak center, and W represents the half-width, half-max of the peak. The denominator of the exponential, R , represents the flatness coefficient (with lower values generating flatter peaks).

However, the lineshape may more closely be represented as a Gaussian profile if (i) the target is highly scattering or (ii) the linewidth of the target is larger than the spectral bandwidth of the spectrometer. For example, in the case of the Hg calibration lamp, light was injected at the focus of the objective lens through 100 μm fused silica fiber, resulting in a lineshape that is more Gaussian in nature.

SHERLOC Calibration Targets

The SHERLOC external calibration target palette is shown in Fig. 4 (upper palette), along with a suite of calibration targets used during thermal vacuum (TVAC) testing (lower palette, not included on the *Perseverance* Rover). The external calibration palette is comprised of 10 targets (clockwise from top left): five spacesuit materials, sourced from NASA Johnson Space Center (JSC) bonded storage: nGimat-coated Teflon fabric, Teflon fabric, Ortho-Fabric, Vectran, polycarbonate spacesuit visor material and opal glass geocache target, aluminum gallium nitride (AlGaN) on sapphire ($\lambda_{\text{max}} \approx 264$ nm) (Texas Tech University), Diffusil diffuser (Opsira GmbH), Mars meteorite SaU 008 (Natural History Museum, London), SiO₂ intensity target (maze) (Applied Image, Inc.), and AlGaN on sapphire ($\lambda_{\text{max}} \approx 340$ nm) (Texas Tech University).

The ground support equipment targets (lower palette of Fig. 4) include (from left to right): highly ordered pyrolytic

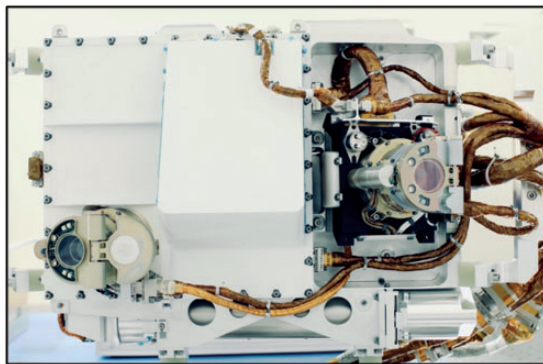


Figure 4. A mosaic image of the SHERLOC external calibration targets (upper palette) and additional calibration targets used during TVAC testing (lower palette) collected by the WATSON imager on the robotic arm of the rover.

graphite (HOPG), Teflon fabric, calcite, Diffusil diffuser (top), first-surface aluminum mirror (bottom), and a BK7 chrome-coated resolution target (Applied Image, Inc.).

During surface operations, the internal AlGa_N (276 nm) (shown in Fig. 5 on the inside of the dust cover) and external calibration targets are measured periodically to characterize changes in the spectral alignment (AlGa_N on sapphire 265 nm and 276 nm (Raman calibration) and 340 nm (fluorescence calibration)), throughput variability (Diffusil diffuser), potential spacesuit material degradation (nGimat fabric, Teflon fabric, Ortho-Fabric, Vectran, polycarbonate), and end-to-end instrument performance and spatial mapping calibration (polycarbonate geocache target, Mars meteorite SaU 008, and maze SiO₂ intensity target). Based on laboratory measurements of the calibration targets, spectral features used for routine wavelength calibration assessment on the Martian surface (including the 252.93 internal laser reflection line and the AlGa_N calibration targets) are not expected to vary with prolonged exposure to UV radiation. Assessment of any potential degradation of the spacesuit material calibration targets will be assessed over the lifetime of the mission, and spectral feature variability will be accounted for in updated wavelength calibrations. Dust is expected to eventually accumulate on the surface of external calibration targets, but dust-clearing events, which have been observed on previous Mars rover missions, may occasionally clean these targets. The 276 nm AlGa_N calibration target located inside of the dust cover is not expected to accumulate dust.

Mercury and Xe lamps (Fig. 3), fed through a 400 and 100 μm fused silica fiber, were used to assess the throughput and alignment of SHERLOC during the initial development and alignment phases of the instrument integration. The Hg lamp provides the most accurate spectral calibration lines over the SHERLOC spectral range. However, in the Raman spectral range, the available lines from the Hg lamp are limited and require additional calibrants. These included the Icelandic spar calcite (CaCO₃), highly ordered pyrolytic

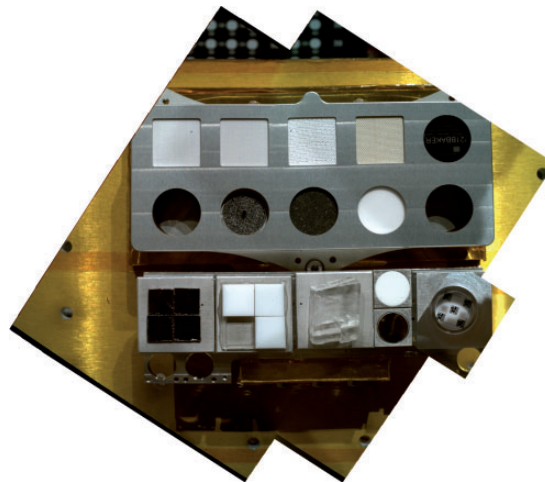


Figure 5. A photograph of the SHERLOC turret assembly before integration with the rover robotic arm. The right boresight is the WATSON color imager, and the left boresight is the ACI imager and spectrometer. The dust cover is open for the spectroscopy boresight in this image.

graphite (HOPG), and Teflon—three materials with well-understood spectral features. While these serve to set the calibration on the ground at room temperature and pressure, the SHERLOC spectrometer requires knowledge of spectral calibration over the environmental conditions it will experience.

Inherent to NeCu DUV lasers are multiple laser lines that can be generated at different output energy levels. While most of these lines have been removed by SHERLOC's laser-conditioning optics, a small fraction of the 252.93 nm line reflected from a target may be observed at an intensity comparable with a strong Raman band. The center wavelength of this atomic emission line is not expected to shift within the operational temperature or pressure ranges. It could therefore operate as an ultra-narrow internal calibrant in all spectral data. In addition, its lineshape can be used to assess the deep UV scattering properties of a target. Given these properties, the 252.93 nm line is expected to be used at the start of surface operations to monitor the wavelength calibration used for SHERLOC measurements. However, the 252.93 line may be lost as a result of a highly reflective or absorbing material, and diminishes with laser age. To mitigate this, a sample of AlGa_N, internally, and Teflon, as a spacesuit material, is located on the SHERLOC calibration target and will provide for a direct comparison to prior spectral data collected during initial calibration efforts.

To calibrate the longer wavelength features, three samples of AlGa_N that were grown on sapphire substrates were included in SHERLOC, two on the SHERLOC calibration palette, and one on the interior lid of the dust cover (Fig. 4). While the AlGa_N targets were grown for specific wavelength ranges, inherent variations in the Al content of

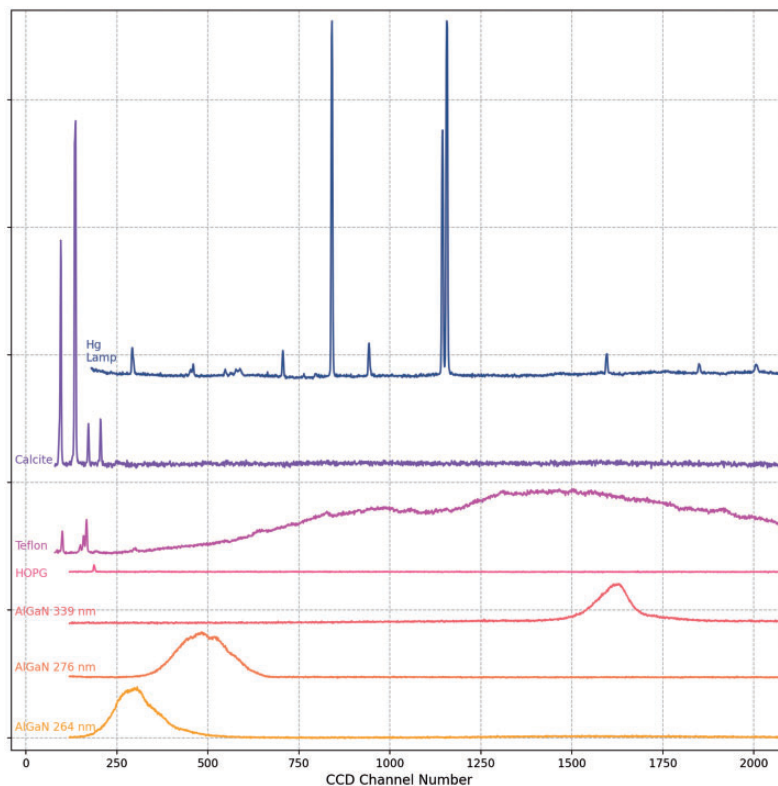


Figure 6. A representative SHERLOC spectrum for each of the targets used in the wavelength calibration. Signal from very high intensity 252.93 nm laser reflection lines on reflective targets and the 253.65 nm Hg emission line have been clipped for readability.

the molecular beam epitaxy process result in non-deterministic spectral peak positions. The initial calibration model enables approximate peak position assignments for the SHERLOC AlGaIn calibration samples, which may be used during operations to verify that the instrument remains in alignment over the course of the mission. All SHERLOC calibration targets will be measured shortly after landing, prior to science investigations, to validate the wavelength calibration model and determine the precise AlGaIn target peak positions, which may differ slightly from the targets described here.

Spectral Calibration Results

The distinct Raman peaks in the HOPG, Teflon, and calcite targets were measured repeatedly during ground-based experiments to assess the performance of the instrument over a variety of operating conditions and to generate an initial wavelength calibration model. Peak positions are extracted from fits to each narrow feature, and a relationship between CCD channel and wavelength is defined.

A representative spectrum from each of the calibration targets used in the wavelength calibration model is presented in Fig. 6. In addition to the calibration targets presented in the SHERLOC Calibration Targets section, emission from an Hg pencil-lamp (UVP, Inc. PenRay Model 90-0012-01) was also measured. The long wavelength

features of the Hg lamp spectra at channel ~ 1845 and ~ 2005 in Fig. 6 are secondary reflections of the 253.65 nm line, which only appear in cases where the SCCD is saturated in the Raman region (the 253.65 nm Hg line, in this example). These features are not included in the wavelength calibration fit.

The initial wavelength calibration data set includes more than 5000 spectra collected over an 18-month period on the ground and during the mission's cruise phase after launch. To simulate surface operation conditions, data were collected under a variety of temperatures, pressures, and laser configurations. The SHERLOC laser pulse width, rep rate, and current may be configured for each measurement to regulate the DUV laser energy deposited at the surface.

A Fermi–Dirac or Gaussian function was fit to all peaks in the calibration data set and compared with the known emission wavelengths for the Hg lamp,¹¹ and the known Raman peak positions of the calcite,¹² Teflon,¹³ and HOPG¹⁴ targets. The observed peak shape is a convolution of the peak's innate broadening (defined by a Poisson distribution) and broadening caused by the image of the beam projected through the slit. Broadening is dominated by the slit function for narrow Raman peaks, and is well-characterized by a Fermi–Dirac distribution. Teflon and AlGaIn targets show a photoluminescence response to the incident laser pulse, resulting in broader peaks distinct from the

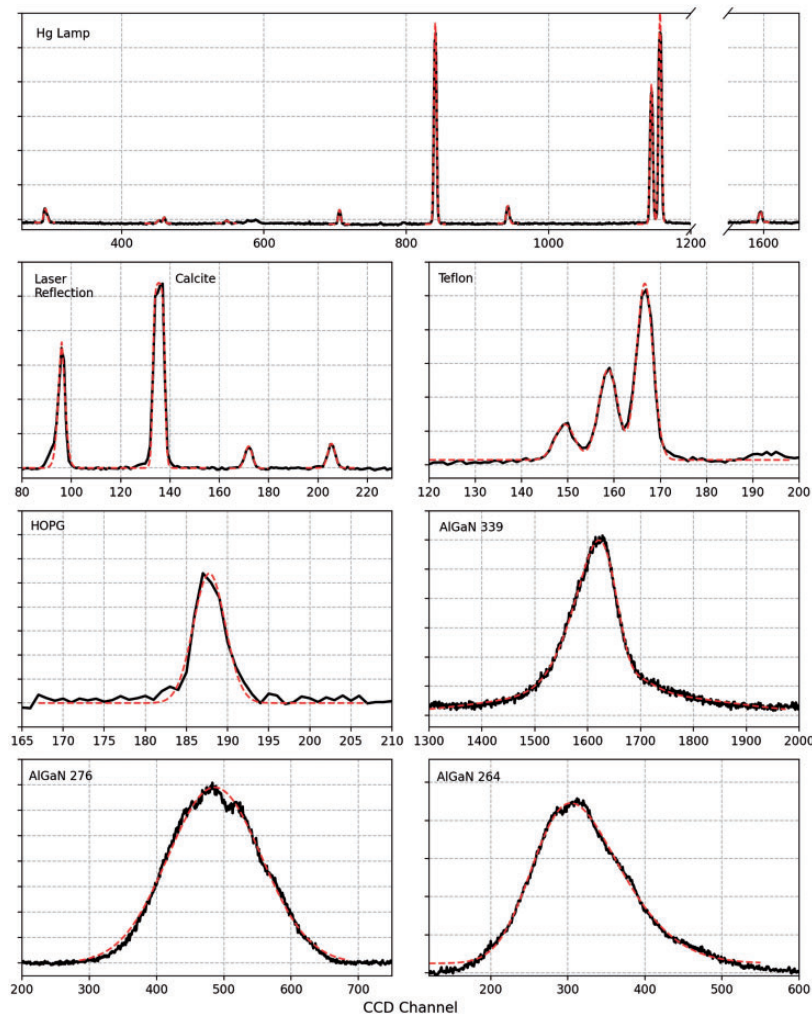


Figure 7. Spectral fits (red traces) and raw data (black traces) for a representative spectrum for each target.

narrow scattering response in other targets, and are therefore more accurately fit by a Gaussian profile. A characteristic peak for each target is presented in Fig. 7, with a Fermi–Dirac or Gaussian fit to each point shown as a red trace. The peak position for the AlGaIn 339 nm feature is determined from a skewed Gaussian profile fit to the spectrum; the slit rotation at longer wavelengths causes the 2D image of the fluorescence intensity distribution to appear asymmetrical on the CCD.

A summary of the peak fitting results is shown in Table I, with the mean, weighted CCD channel associated with each peak, along with the mean peak FWHM and the number of suitable spectra included in each peak fit. The FWHM is observed to increase at longer wavelengths in the Hg emission peak fit results, as shown in Fig. 8; the rotated slit associated with this part of the CCD subtends more pixels, resulting in an apparent larger spectral image, only partially offset by the smaller spectral bin size at longer wavelengths. In Fig. 8, atomic emission lines from the Hg lamp spectrum that are unaffected by the saturated

253.65 nm line were included, along with the calcite spectrum 252.9 line.

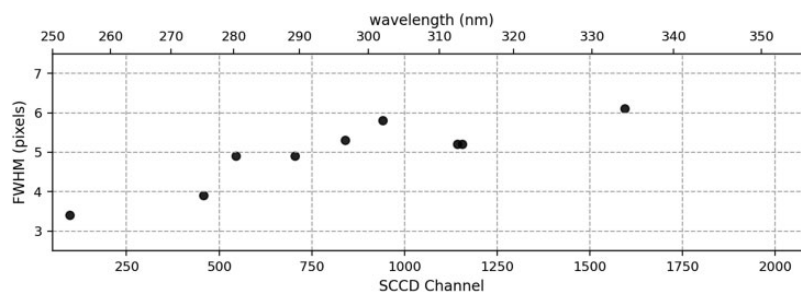
A weighted second-order polynomial is fit to the Raman and fluorescence CCD regions separately. Data points are weighted by the SNR of the peak, with outlier points removed from the fit, determined by a high FWHM (greater than two times the median FWHM) or low peak signal (peak amplitude is less than two times the standard deviation of dark frame counts). The resulting wavelength calibrations are presented in Fig. 9. The blue dashed line and red dashed line represent the Raman and fluorescence segments of the wavelength calibration model, respectively. The size of each point in Fig. 9 represents the weighting factor, and the color of the points represents the calibration target of the associated peak (using the same color scheme as in Fig. 6).

The wavelength range of the SHERLOC spectrometer extends from 249.9 nm to 353.6 nm, and matches the initial optical model of the SHERLOC spectrometer generated prior to assembly of the instrument. Figure 10 shows the

Table I. A summary of the peak fitting results and wavelength assignments for all spectral peaks used in the SHERLOC wavelength calibration.

Target	Wavelength (nm)	Wavenumber (cm ⁻¹)	Fit results			
			CCD channel	FWHM	# Spec.	Residual to fit (cm ⁻¹)
Hg lamp	253.65	801	107.48 ± 0.0	4.9	2	2.0
Hg lamp	265.20	2518	292.2 ± 0.9	5.9 ^a	142	-11.6
Hg lamp	275.28	3899	458.5 ± 0.8	3.9	105	-2.9
Hg lamp	280.35	4556	545.8 ± 0.6	4.9	10	-2.3
Hg lamp	289.36	5666	705.1 ± 1.0	4.9	133	2.2
Hg lamp	296.70	6521	840.6 ± 0.7	5.3	156	-4.8
Hg lamp	302.15	7129	941.9 ± 1.0	5.8	134	1.5
Hg lamp	312.57	8232	1144.3 ± 0.7	5.2	98	-0.4
Hg lamp	313.17	8294	1156.4 ± 0.5	5.2	98	-0.7
Hg lamp	334.15	10299	1594.7 ± 0.8	6.1	134	2.1
Calcite	255.45	1079	136.2 ± 0.3	4.4	441	-5.1
Calcite	257.76	1430	172.6 ± 0.4	3.6	441	-6.3
Calcite	259.87	1745	206.2 ± 0.4	3.5	441	-8.0
Teflon	256.34	1215	149.2 ± 0.3	5.2	568	4.5
Teflon	256.87	1295	158.4 ± 0.3	5.2	569	-5.1
Teflon	257.43	1379	166.3 ± 0.3	4.6	570	3.5
HOPG	258.80	1585	188.0 ± 0.4	4.5	1068	2.7
AlGaIn	263.95	2339	270.6 ± 1.5	132	18	N/A
AlGaIn	276.33	4037	475.9 ± 1.6	169	247	N/A
AlGaIn	339.02		1704.0 ± 8.7	96	66	N/A

^aThe average FWHM of the 265.20 Hg emission line is high due to the nearby 253.65 nm line, which is nearly always saturated in these measurements, skewing the peak shape of the 265.20 line.

**Figure 8.** The average FWHM of Hg emission lines and the 252.93 nm laser reflection line, showing the reduced resolution of the spectrometer at higher wavelengths.

results of the optical model (red dashed trace) compared with the empirical wavelength calibration (black trace) using the methods described above. The error in the calibration is presented in Fig. 10, showing the residual of the average peak positions relative to the wavelength calibration model.

Discussion

Over 5000 spectra were evaluated to calculate the SHERLOC wavelength calibration model over a variety

of environmental conditions within the nominal operation range of the instrument on Mars (approximately -40°C to 40°C). Some wavelength calibration variability is expected due to environmental changes,^{15,16} and slight wavelength shifts on the SCCD have been identified in test data. A linear spectral shift along the dispersion axis of the spectrometer has been observed over the 80°C temperature range, on the order of a few pixels. A simple correction factor (k) may be applied to the wavelength calibration Eq. 2 to accommodate this thermal

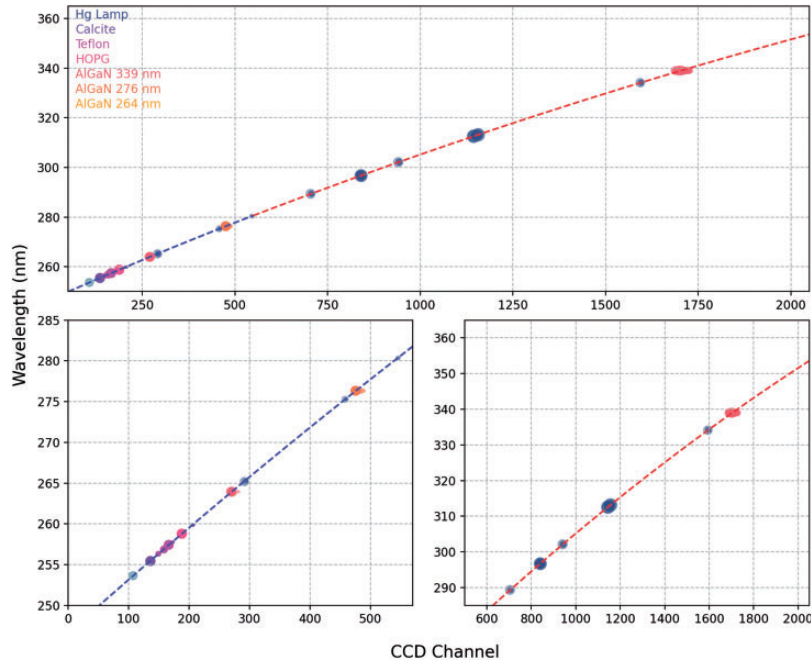


Figure 9. Wavelength calibration to known peaks in the Raman and fluorescence regions. The upper plot shows the combined calibration fit to the data. The lower left plot shows the Raman calibration segment and the lower right plot shows the fluorescence region calibration. AlGaIn peak assignments were determined from the results of the wavelength calibration.

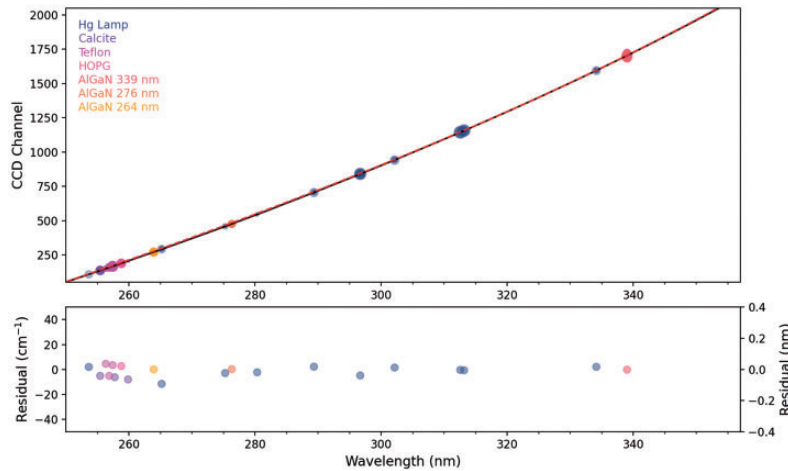


Figure 10. The wavelength calibration (black trace) compared with the modelled wavelength calibration from the initial optical model of the SHERLOC system (red trace).

effect; the value of k is derived from the position of internal calibration peaks measured before and after each science measurement, described in the Surface Operations Calibration section. The SCCD thermal environment is maintained over the duration of a spectral map acquisition through the use of a phase change material heatsink, which stabilizes the temperature for more than an hour during operations. Wavelength calibration variability along the vertical axis of the SCCD is determined to be less than the resolution of the spectrometer

within the expected SHERLOC temperature and pressure operational ranges.

The segmented wavelength calibration for SHERLOC surface operations is defined by Eq. 2, where x represents the CCD channel number (or a fraction of a CCD pixel), and k represents the thermal correction factor. A segmented quadratic wavelength calibration equation was empirically determined to minimize residuals of the peak-fitted measured data, with results in close agreement with the expected wavelength positions on the CCD predicted

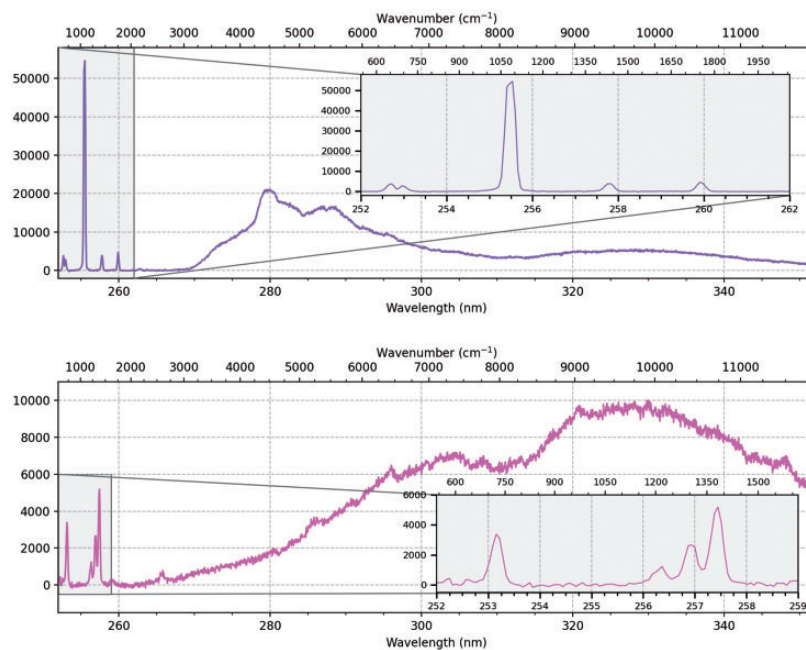


Figure 11. The SHERLOC calibration model applied to calcite (above) and Teflon (below) targets.

by the SHERLOC ray trace model. The first and last 50 pixels on the SHERLOC SCCD (pixel number 1–50 and 2098–2148) are not light-sensitive, but these inactive pixels are considered in the wavelength calibration equation below

$$\lambda(\text{nm}) = \begin{cases} (-7.85 \times 10^{-6})(x+k)^2 + (6.62 \times 10^{-2})(x+k) + 246.6, & x < 500 \\ (-5.66 \times 10^{-6})(x+k)^2 + (6.34 \times 10^{-2})(x+k) + 247.5, & x \geq 500 \end{cases} \quad (2)$$

An example of this calibration model applied to the Teflon and calcite calibration targets, measured at approximately -10°C during a system thermal test, is presented in Fig. 11.

Surface Operations Calibration

The internal AlGaIn target (276 nm) is measured during laser conditioning and before and after each SHERLOC spectroscopy measurement activity to provide an assessment of potential degradation of the instrument throughput or spectral alignment every time the instrument performs a spectral measurement. Once data are downlinked, automated ground data processing software tools will evaluate the peak locations of the Rayleigh-scattered 252.9 nm laser reflection and the 276 nm AlGaIn peak, and will notify the SHERLOC team if the spectral alignment has drifted

beyond expected tolerances, within one pixel (less than $13.5\ \mu\text{m}$) for the narrow 252.9 laser reflection line and within 20 pixels for the broad AlGaIn feature. This may allow more timely measurements of the external calibration target suite to update the wavelength calibration model, if necessary.

Conclusion

We evaluated all SHERLOC data from instrument alignment, integration and testing, launch, and cruise phases of development, and generated a wavelength calibration model of the spectrometer necessary for the characterization of minerals and organics during rover operations on the surface of Mars. Narrow-band peak positions of calibration targets measured by SHERLOC were fit with Fermi–Dirac or Gaussian profiles, compared with known reference wavelengths, and a relationship between CCD channel and wavelength was defined.

The wavelength calibration model employs a segmented, weighted second-order polynomial fit to all suitable peak positions from Teflon, calcite, AlGaIn, and HOPG calibration targets, and an Hg lamp, which sufficiently covers the entire wavelength range. The spectrometer is sensitive from 249.9 nm to 353.6 nm, and stable over operational temperatures and pressures, meeting the scientific requirements of a SHERLOC investigation.

Periodic measurements of the internal AlGaIn calibration target, as well as targets on the SHERLOC calibration palette, will allow for refinements to the instrument wavelength calibration model during operations on Mars. In the

event of calibration target degradation or dust coverage, solar measurements may be performed to recalibrate SHERLOC using the known positions Fraunhofer lines.

In addition to the missions' baseline science objectives achieved through DUV Raman and fluorescence spectroscopy, SHERLOC could potentially also operate as a UV emission spectrometer, for which an accurate wavelength calibration model would be critical.

Acknowledgments

The research was carried out at the Jet Propulsion Laboratory, California Institute of Technology, under a contract with the National Aeronautics and Space Administration (NASA). We greatly appreciate useful discussions with Shiv Sharma. The authors acknowledge support from the Mars 2020 Navcam imaging team for the image featured on the cover of this issue.





Declaration of Conflicting Interests

The author(s) declared no potential conflicts of interest with respect to the research, authorship, and/or publication of this article.

Funding

The author(s) disclosed receipt of the following financial support for the research, authorship, and/or publication of this article: This project was funded by the SHERLOC instrument on the Mars 2020 rover, under funding from NASA Headquarters.

ORCID iDs

Kyle Uckert  <https://orcid.org/0000-0002-0859-5526>
 Luther W. Beegle  <https://orcid.org/0000-0002-4944-4353>
 Ryan S. Jakubek  <https://orcid.org/0000-0001-7880-9422>
 Ryan D. Roppel  <https://orcid.org/0000-0002-1782-1388>

References

1. K.A. Farley, K.H. Williford, K.M. Stack, R. Bhartia, A. Chen, et al. "Mars 2020 Mission Overview". *Space Sci. Rev.* 2020. 216(142): 1–41.
2. R. Bhartia, L.W. Beegle, L. DeFlores, W. Abbey, J. Razzell Hollis, et al. "Perseverance's Scanning Habitable Environments with Raman and Luminescence for Organics and Chemicals (SHERLOC) Investigation". *Space Sci. Rev.* 2021. 217: 58. doi: 10.1007/s11214-021-00812-z.
3. A.C. Allwood, L.A. Wade, M.C. Foote, W.T. Elam, J.A. Hurowitz, et al. "PIXL: Planetary Instrument for X-ray Lithochemistry". *Space Sci. Rev.* 2020. 216(134): 1–132.
4. R.C. Moeller, L. Jandura, K. Rosette, M. Robinson, J. Samuels, et al. "The Sampling and Caching Subsystem (SCS) for the Scientific Exploration of Jezero Crater by the Mars 2020 Perseverance Rover". 2021. *Space Sci. Rev.* 217(5): 1–43.
5. J.F. Bell, J.N. Maki, G.L. Mehall, M.A. Ravine, M. A. Caplinger, et al. "The Mars 2020 Perseverance Rover Mast Camera Zoom (Mastcam-Z) Multispectral, Stereoscopic Imaging Investigation". 2021. *Space Sci. Rev.* 217(24): 1–40.
6. R.C. Wiens, S. Maurice, S.H. Robinson, A.E. Nelson, P. Cais, et al. "The SuperCam Instrument Suite on the NASA Mars 2020 Rover: Body Unit and Combined System Tests". *Space Sci. Rev.* 2021. 217(4): 1–87.
7. W.J. Abbey, R. Bhartia, L.W. Beegle, L. DeFlores, V. Paez, et al. "Deep UV Raman Spectroscopy for Planetary Exploration: The Search for in situ Organics". *Icarus.* 2017. 290: 201–214.
8. J. Razzell Hollis, D. Rheingold, R. Bhartia, L.W. Beegle. "An Optical Model for Quantitative Raman Microspectroscopy". *Appl. Spectrosc.* 2020. 74(6): 684–700.
9. K.S. Edgett, R.A. Yingst, M.A. Ravine, M.A. Caplinger, J.N. Maki, et al. "Curiosity's Mars Hand Lens Imager (MAHLI) Investigation". *Space Sci. Rev.* 2012. 170(1–4): 259–317.
10. J.A. Hoffnagle, C.M. Jefferson. "Measured Performance of a Refractive Gauss-to-Flattop Reshaper for Deep-UV Through Near-IR Wavelengths". *Proceedings Volume 4443: Laser Beam Shaping II. International Society for Optics and Photonics.* 2001. 4443: 115–124.
11. C.J. Sansonetti, M.L. Salit, J. Reader. "Wavelengths of Spectral Lines in Mercury Pencil Lamps". *Appl. Opt.* 1996. 35(1): 74–77.
12. J. Razzell Hollis, S. Ireland, W. Abbey, R. Bhartia, L.W. Beegle. "Deep-Ultraviolet Raman Spectra of Mars-Relevant Evaporite Minerals Under 248.6 nm Excitation". *Icarus.* 2021. 357: 114067.
13. J. Koenig, F. Boerio. "Raman Scattering and Band Assignments in Polytetrafluoroethylene". *J. Chem. Phys.* 1969. 50(7): 2823–2829.
14. Y. Wang, D.C. Alsmeyer, R.L. McCreery. "Raman Spectroscopy of Carbon Materials: Structural Basis of Observed Spectra". *Chem. Mater.* 1990. 2(5): 557–563.
15. R.S. Jakubek, M.D. Fries. Calibration of Raman Wavenumber in Large Raman Images Using a Mercury-Argon Lamp". *J. Raman Spectrosc.* 2020. 51: 1172–1185.
16. S. Fukura, T. Mizukami, S. Otake, H. Kagi. "Factors Determining the Stability, Resolution, and Precision of a Conventional Raman Spectrometer". *Appl. Spectrosc.* 2006. 60(8): 946–950.